Effect of creep loading on the oxygen diffusion of Ti6242S at 650°C

K. Cavé, D. Texier, S. Vallot, N. Chanfreau, E. Fessler, M. Dehmas, Daniel Monceau, Dominique Poquillon

Effect of creep loading on the oxygen diffusion of Ti6242S at 650°C

K. Cavé [a,b,c], D. Texier [b], S. Vallot [b], N. Chanfreau [a], E. Fessler [c], M. Dehmas [a], D. Monceau [a], D. Poquillon [a]

[a] CIRIMAT, Toulouse INP, Université Toulouse 3 Paul Sabatier, CNRS, Université de Toulouse, 4 Allée Emile Monso, BP 44362, 31030, Toulouse, Cedex 4, France
[b] Institut Clement Ader (ICA) - UMR CNRS 5312, Université de Toulouse, CNRS, INSA, UPS, Mines Albi, ISAE-SUPAERO, Campus Jarlard, 81013, Albi, Cedex 09, France
[c] SAFRAN Aircraft Engines, Rond-Point René Ravaud, 77550, Moissy-Cramayel, France

A B S T R A C T

The influence of low and steady loading on the oxidation behaviour and oxygen diffusion within Ti6242S was investigated at 650 °C in air. Electron probe microanalyser (EPMA), secondary-ion mass spectrometry (SIMS) and high energy synchrotron X-ray diffraction (S-XRD) were used to quantify the oxygen distribution within the oxygen-enriched layer beneath the external oxide scale. Rietveld and peak by peak methods were used to evaluate the average response versus the crystal-oriented response of this diffusion process under load. Interestingly, a thermo-mechano-chemical coupling occurs during the creep-oxidation experiment even for moderate applied stresses (25-70 MPa) and demonstrates: (i) a decrease of the oxygen concentration at the metal/oxide interface, and (ii) a curvature change of the oxygen diffusion profile with load application. A qualitative thermo-mechano-chemical approach is proposed to model the modification of the diffusion law of the oxygen within Ti6242S due to application of a mechanical loading to explain observed experimental results.

Ti6242S is used for the manufacture of compressor discs in aerospace application due to better high temperature mechanical properties and better oxidation resistance compared to Ti-6Al-4V [1]. Its oxidation behaviour is yet a limiting factor in the design of structural components above 450 °C primarily due to the formation of an oxygen-enriched layer (ORL) beneath the oxide layer. The ORL demonstrates a brittle behaviour [2–4], detrimental to fatigue lifespan [5]. The extension and oxygen distribution within the ORL arise from the high solubility limits of oxygen within both α and β phases. Several authors have investigated the oxidation behaviour of Ti6242S without applied loading [2,6–8]. However, aeronautical components are generally submitted to mechanical loading during operative life. Therefore, understanding how an external loading could influence the oxidation behaviour is a necessary step in the design of aeronautical structural components to improve their lifespan.

Different characterisation techniques are available to probe either the local oxygen content with energy dispersive spectroscopy (EDS) [9], electron probe microanalysis (EPMA) [7,10–13], secondary-ion mass spectrometry (SIMS) [14], electron energy loss spectroscopy (EELS) [9], atom probe tomography (APT) [15] or the local mechanical response of the material within the ORL related to a given oxygen content using nanoindentation [12,13] and microindentation [6,7,16–18]. Oxygen insertion also leads to α-titanium lattice expansion which can be characterised by diffraction techniques using synchrotron radiation [17,19]. In service, Ti alloys can be exposed at 450 °C to 550 °C for several hours. For such conditions, the ORL spreads within tens of micrometres with an oxygen distribution profile gradually decreasing from [25–33] at%. at the metal/oxide interface to the nominal oxygen composition in the core. The large oxygen concentration gradient in the vicinity of the metal/oxide interface and difficulties in accurate positioning of spectroscopic analyses at the sub-micron scale lead to difficulties to accurately assess oxygen concentration at the metal/oxide interface. This concentration is particularly important for the identification of the coefficient of diffusion. While EDS, SIMS, EPMA and other spectroscopic analyses inform on the local oxygen content, quantitative analyses find difficulties due to surface contamination related to instantaneous formation of a native nanometric TiO_2 oxide scale after sample preparation. Oxygen distribution profiles and local mechanical property gradients [6,7,16–18,20] were reported in the literature. Diffusion profiles can be generally interpreted using Fick's law. However, the influence of external loading during high-temperature Ti alloys oxidation on oxygen distribution within ORL has been limitedly studied and requires further

research. An increase in oxidation rate was observed at the early stage of oxidation under bending loading at high temperature for Ti-6Al-4V and high-purity titanium materials [21]. This increase in oxidation rate was associated with thicker external oxides but the effect of tensile loading was not clear on the ORL formation.

The aim of this work is to investigate the thermo-mechano-chemical coupling operating during creep at elevated temperature of Ti6242S under oxidative atmosphere without cracking either the oxide scale or the ORL. We investigated the effect of static tensile stresses with moderate stress levels (25-70 MPa) on the oxygen diffusion within the ORL using EPMA, SIMS, and synchrotron X-Ray diffraction (S-XRD).

The as-received Ti6242S exhibits a Widmanstätten microstructure with α lamellae (2-3 μm) and α colonies with average width of 30 μm (Please see Ref. [22] for additional information). The measured chemical composition in mass% is 5.8Al, 2.0Sn,4.3Zr, 1.9Mo, 0.1Si, 0.02Fe, 0.12O, 0.002N and balance Ti.

Flat creep samples with a gauge length of 30 mm and a gauge section of 5 × 2 mm^2 were used for oxidation under loading. The same surface finish was applied for creep and non-loaded samples (P600 SiC grit paper). The non-loaded sample considered as a reference, was oxidised 120 h at 650 °C in a Nabertherm furnace with forced convection. Oxidation under loading at 650 °C was performed on a static creep test rig under laboratory air and under stresses equal to 25 and 70 MPa for 120 h These stress levels were chosen not to induce failure and spallation of the oxide layer during loading, as confirmed by surface and cross-section observations (ThermoFisher Scientific Quanta 450 scanning electron microscope (SEM)). Heating was obtained using a halogen furnace and temperature was measured at the extremities of the gauge length using welded K-type thermocouples. The total deformation measured for 25 (resp. 70) MPa sample is 0.2 % (resp. 0.6 %).

Four samples were extracted from oxidised specimens to analyse oxygen distribution within the ORL, *i.e.*, S-XRD, EPMA and SIMS analyses. For EPMA, samples were first electroplated using copper to preserve the external oxide layer during sample preparation, then cross sectioned and ground with SiC grit papers down to 1 μm diamond particles. The oxygen concentration within the ORL was measured down to a depth of 80 μm using EPMA on a CAMECA SXFive at 10 keV with a measurement step of 1 μm (3 profiles per condition). Oxygen as well as nitrogen intensity profiles were also measured using SIMS on a CAMECA IMS 4FE6. A Cs+ primary ion beam of 10 kV impact energy was employed at a current density of 370 nA. The sputter rate was determined by repeated depth measurement using an Olympus LEXTOLS5100 laser scanning confocal microscope. Increase in roughness inherent to sputtering limited characterisations to be carried out over approximately 20 μm for SIMS analyses. Height maps were then exploited using Gwyddion software [23].

EPMA analyses demonstrate the role of an external load on the oxygen profiles, *i.e.*, on the concentration at the metal/oxide interface and on the apparent diffusion coefficient of O within Ti, D_{app} (Fig. 1(a)). Oxygen profiles follow a Fick's law considering the case of diffusion of oxygen in titanium with a semi-infinite thickness and a constant oxygen concentration within Ti at the metal/oxide interface, C_s:

$$\frac{C(x) - C_0}{C_s - C_0} = 1 - \mathrm{erf}\left(\frac{x}{\sqrt{4D_{app}t}}\right) \quad (1)$$

with C_0 the bulk concentration, $C(x)$ the oxygen concentration at a depth x and exposure duration t. The calculated parameters of the model using a least square optimisation are reported in Table 1. A decrease of C_s value was found with the application of an external loading, enhanced with the applied stress. Similarly, the curvature of the diffusion profile evolved with the applied stress, leading to an increase of the effective diffusion coefficient. At 70 MPa, the diffusion coefficient is nearly two times larger than the one in non-load condition.

Oxide thicknesses were also measured (Table 1). The thickness of oxide for loaded samples seems independent of the applied load value considering scattering. Interestingly, the thickness is greater for unloaded sample. The greater air speed in furnace with forced convection compared to furnace with natural convection used for loaded samples as in Ref. [24] can explain these observations. We evaluate also the ORL

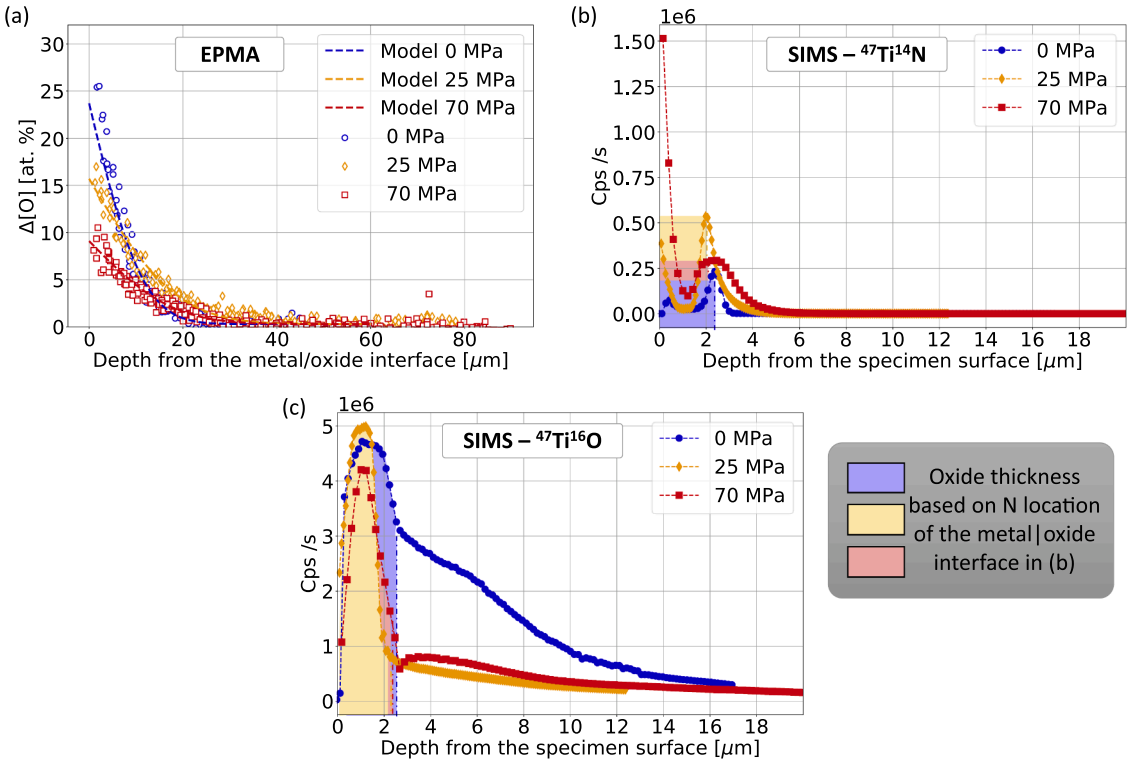

Fig. 1. EPMA (a), SIMS for $^{47}Ti^{14}N$ (b) and $^{47}Ti^{16}O$ experimental data(c)). Fitting of EPMA results are also plotted in (a). Depth data for $^{47}Ti^{16}O$ were re-adjusted by using the position of the maxima for $^{47}Ti^{14}N$.

Table. 1
Diffusion coefficient and *Cs* values identified from EPMA and synchrotron analyses. The accuracy of the diffusion coefficient values was estimated considering the scattering in experimental oxygen profiles with different least-square method fittings.

σ [MPa]	0	25	70
D_{app} x 10^{16} [$m^2.s^{-1}$]	0.94 ± 0.4	2.5 ± 0.3	2.2 ± 0.6
C_s [at. %]	23.7 ± 2	15.7 ± 2	9.1 ± 2
e_{oxyde} [μm]	2.8 ± 0.7	1.9 ± 0.3	2.0 ± 0.2
ORL EPMA [μm]	23 ± 2	36 ± 1	31 ± 4
$D_{synchrotron\text{-}a}$ x 10^{16} [$m^2.s^{-1}$]	1.7 ± 0.1	3.2 ± 0.1	3.8 ± 0.1
$D_{synchrotron\text{-}c}$ x 10^{16} [$m^2.s^{-1}$]	1.8 ± 0.1	3.3 ± 0.1	4.6 ± 0.1

extension with a cut criteria proposed by Shenoy et al. [6]. These authors defined the brittle-to-ductile transition concentration of oxygen in titanium at 0.5 at. %. ORL extension was found greater for crept samples (Table 1).

SIMS profiles evidenced the occurrence of nitrogen at the metal/oxide interface more prominent with the external load and related with a minimum of oxygen content (Fig. 1(b) and (c) after adjustment). In addition, the position of the nitrogen maxima is coherent with oxide thickness measured in Table 1. This finding is in accordance with the literature, reporting that nitrogen decreases the oxygen concentration at the metal/oxide interface by nitride formation or by competitive interstitial sites occupation [9,25]. Both the nitride precipitates and the larger interstitial site occupancy by nitrogen act as a diffusion barrier for oxygen and subsequently decrease oxygen dissolution within the Ti6242S [15]. In addition, the oxide scale growth is slower in the presence of nitrogen at the metal/oxide interface. Moreover, a modification of the oxygen profile can be observed in/beneath the oxide scale with load application in Fig. 1 (c).

S-XRD measurements were performed on the P21.2 beamline at the Deutsches Elektronen-SYnchrotron (DESY) in Hamburg. A schematic illustration is presented in Fig. 2 to clarify the experimental method for sample positioning, scanning and data analysis. Sample surface was ground with SiC paper up to P600 grit paper and a special attention was paid on the parallelism of the faces.

The sample was carefully positioned and slightly tilted so that the beam line and the sweep direction are parallel to the metal/oxide interface. Samples were illuminated by a monochromatic X-ray beam of 82 keV (wavelength of 0.015028 nm) with a cross section of 7 × 2 μm^2. During X-ray radiation, the sample was swept parallel to the metal/oxide direction along 1 mm at each analysed depth to increase the analysis volume. Diffraction analyses were performed each micrometre from the external scale to the sample core. Calibration of the sample distance to the 2D detector were done using a TiC calibrant. 2D diffractograms were then angularly or partially integrated to obtain 1D diffractograms, analysed using FullProf software [26]. The variation of α-titanium lattice parameters in ORL was calculated using Rietveld refinement for fully integrated rings and peak by peak method for partially integrated rings.

The variation of the mean lattice parameters *c* and *a* of the hexagonal close-packed α-titanium phase within the ORL was assessed as a function of the distance from the metal/oxide interface (Fig. 3). These

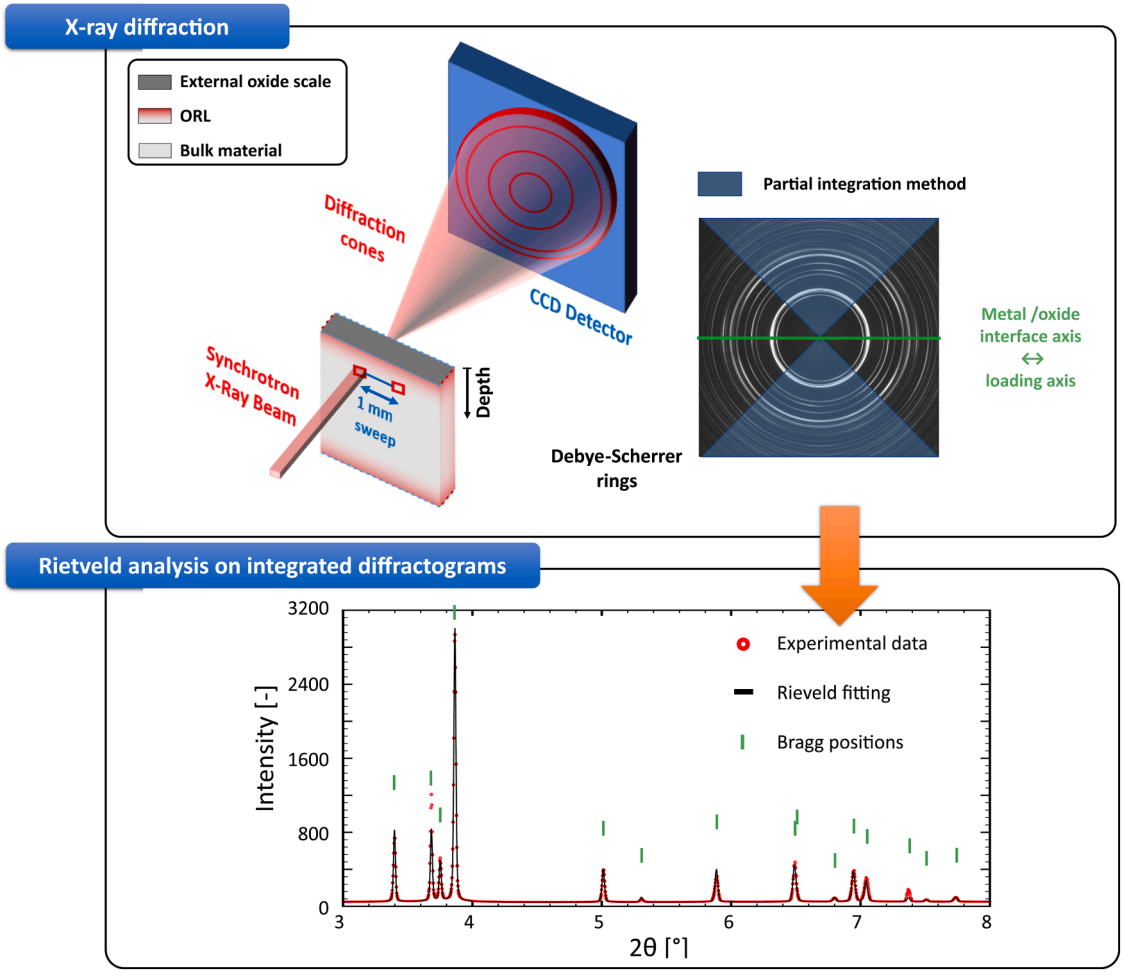

Fig. 2. Schematic illustration S-XRD measurements Rietveld analyses on fully integrated diffractograms. Partial integration method is also illustrated on Debye-Scherrer rings and used for peak by peak method.

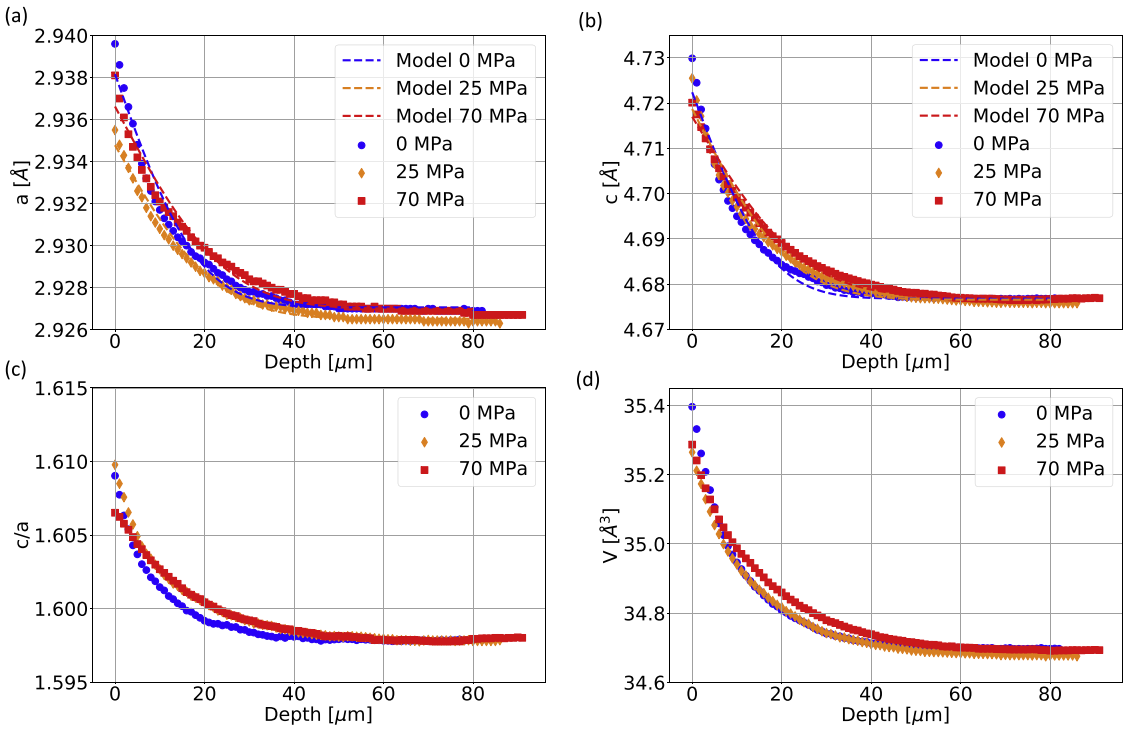

Fig. 3. Variation of the lattice parameters of the α-titanium phase as a function of the metal/oxide interface: *a* (a), *c* (b), *c*/*a* ratio (c) and, volume (d).

measurements aimed at calculating in a similar way the variation of the *c*/*a* ratio and the lattice volume. An increase in all the crystallographic parameters was found with the increase in oxygen content, as already reported in the literature [17,19]. Interestingly, an anisotropic expansion of the crystallographic structure due to oxygen insertion is illustrated by the evolution of the *c*/*a* ratio, *c* being 1.6 times more sensitive than *a*. The *c*/*a* ratio is nearly 1.609 at the oxide/metal interface and different for loaded and non-load samples while it stabilises at 1.598 far from the ORL. These ratio are close to values from Ref. [27] observed on Ti-O systems with various oxygen contents. The non-loaded sample exhibits higher lattice parameters, *i.e.,* *a*, c, and volume, at the metal/-oxide interface compared to the crept samples. As for the oxygen distribution, the curvature of the crystallographic parameter profiles decreases with the application of the external loading. A linear relation between local oxygen content and *a* & *c* lattice parameters (Vegard's law) did not to reproduce the measured evolutions, contrary to evolutions reported in Ref. [17] (Fig. 3 (a) and (b)).

The different complementary analyses evidenced a decrease in oxygen content and lattice parameter values at the metal/oxide interface under stress associated with a modification of oxygen and lattice parameters profile curvature. Furthermore, the presence of nitrogen in the vicinity of or at the metal/oxide interface was also evidenced and affected by the external load. D_{app} values for unloaded sample obtained from both techniques are in agreement with literature [2,6,24,28]. Differences in diffusion coefficients with load increase shown in the present paper is with the scatter reported in the open literature. Considering this scattering, it is difficult to conclude on loading effect on oxygen profile. We investigated the influence of local α-cells orientation on lattice expansion by partially integrating Debye-Scherrer rings (see Figs. 2 and 4 (a)) to complete Rietveld method. From the best of the authors' knowledge, such an approach was never reported to study α-titanium cells expansion within ORL. α-lattice parameter values were calculated using {0002} (resp. $\{10\bar{1}0\}$) position for *c* (resp. *a*) parameter and Bragg relationship using the peak by peak method [29]. This method allows us to study the orientation influence on α-cell expansion by considering particular α-cell population as only one diffraction peak is used for lattice calculations contrary to Rietveld method's, which is an "average" analysis as all peaks are considered. Two α-cell populations are studied: α cells with *c* axis nearly parallel (1) and perpendicular (2) to the metal/oxide interface, *i.e.*, the loading direction. The results of the peak by peak method is illustrated in Fig. 4 (a) and (b) for the unloaded sample and highlights that the Rietveld results are included between the two considered populations. The maximum values of lattice parameters at the metal/oxide interface and the shape of their profile were found to be sensitive to the considered populations.

For unloaded sample, the expansion on the *a* and *c* axis seems easier if those directions are parallel to the interface metal/oxide, see Fig. 4 (a) and (b). This observation is also testable for loaded samples. Interestingly, the load application leads to a decreased expansion on both directions *a* and *c* if those directions are close to the parallel to the loading direction (see Fig. 4 (c) & (f)). If the directions *a* and *c* are close to the perpendicular to the loading direction, application of 70 MPa leads to a greater expansion on both directions (see Fig. 4 (d) & (e)). These results deserve more investigations but demonstrate the influence of local texture, and thus local crystallographic orientation, for determining diffusion coefficients. With these new considerations, the loading influence on the lattice parameter gradient within ORL remains difficult to assess. This relative influence may be explained by the low applied loads. Regarding α-cell expansion with oxygen [16,27,30] and nitrogen [31] content in literature, we observe that both parameters *a* and *c* obtained with Rietveld method vary slightly in this study compared to local oxygen content.

The various analyses carried out seem to highlight two effects never observed for such moderate applied stresses (25-70 MPa). External loading had a concomitant effect on (i) the oxygen and nitrogen concentrations at the metal/oxide interface and (ii) the shape of the diffusion profile and extension of the ORL due to a larger apparent diffusion coefficient. It is not currently possible to dissociate the relative contributions of the apparent diffusion coefficient and of the nitrogen segregation on the oxygen concentration at the metal/oxide interface. Fig. 5 is a schematic illustration of the qualitative contribution of applied loading on the stress and oxygen distribution in the ORL due to the concomitant action of the elastic gradient $J_{O-Mechan}$ and of the oxygen

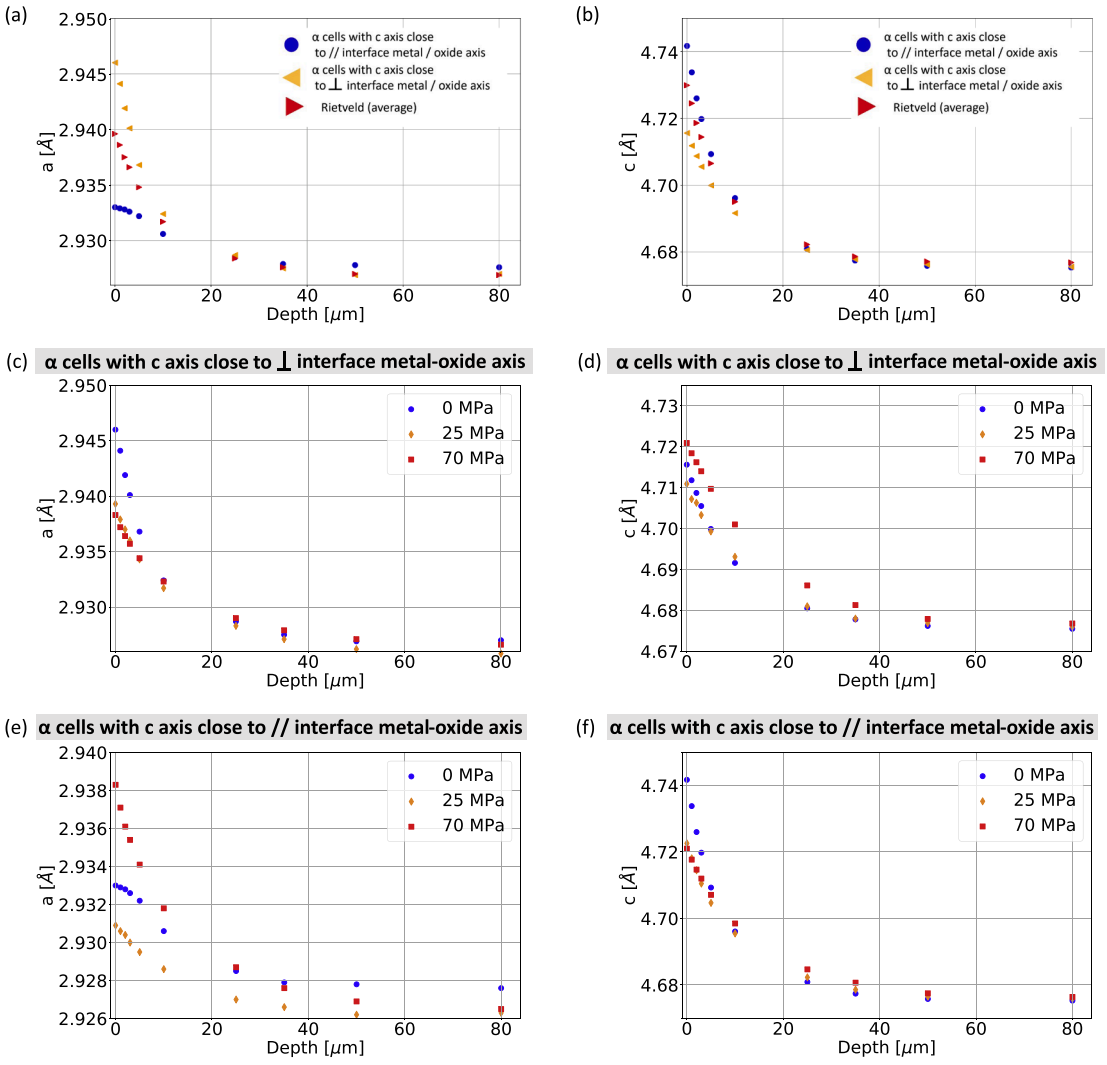

Fig. 4. Comparison of peak by peak and Rietveld methods on parameters *a* (a) and *c* (b) for unloaded sample. Influence of tensile stress on peak by peak results considering different α-cell populations for parameters *a* (c & e) and *c* (d & f).

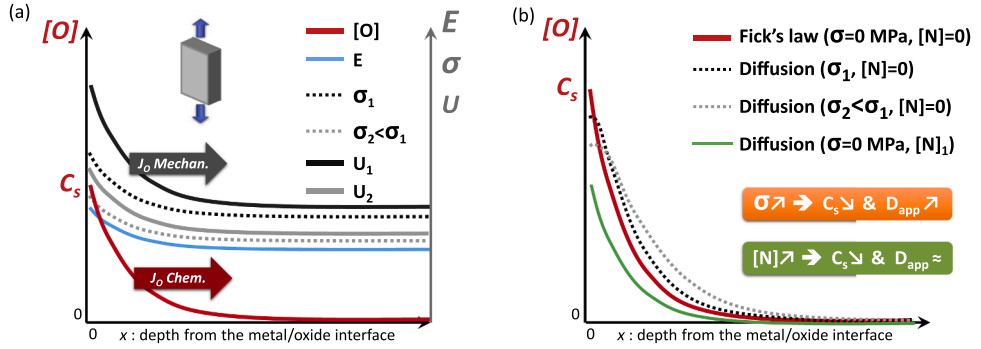

Fig. 5. Schematic illustration of oxygen profile, elastic energy *U*, Young modulus *E* and stress level σ within ORL (a) and how oxygen profile can be influenced by nitrogen presence and/or load application (b).

flux $J_{O\text{-}Chem}$. For the first effect, we only focus on the elastic mechanical contribution. In the presence of an external stress, the hydrostatic stress influence the global equilibrium, as reported for hydrogen diffusion in stressed zirconium [32]. The increase of oxygen content in titanium is known to increase Young Modulus *E* values, as reported by Baillieux [33]. In ORL, this leads to a Young Modulus and stress gradients induced by a core-shell effect, as illustrated in Fig. 5 (a). This core-shell effect will progressively unload the sample core with a growing ORL. An additional contribution due to the elastic gradient $J_{O-Mechan}$ can be added in the Fick's law. Qualitatively, this additional contribution leads to a decrease of the oxygen profile curvature as illustrated in Fig. 5 (b) and then to an increase of D_{app} and to a decrease of C_s with increased exposure time. The dissolved nitrogen or nitrides formation under the oxide scale will only influence C_s (see Fig. 5 (b)).

To summarize, this study highlights the effects of a moderate load on the diffusion of O within Ti with (i) a decrease of the oxygen concentration at the metal/oxide interface due to nitrogen segregation and/or nitride formation, (ii) a modification of the shape of the oxygen and lattice parameters (*a* & *c*) profiles due to a larger effective diffusion coefficient value under moderate loading, and (iii) an anisotropic evolution of the lattice parameters (orientation of α-titanium cells regarding the metal/oxide interface).

Declaration of Competing Interest

The authors declare the following financial interests/personal relationships which may be considered as potential competing interests: Damien TEXIER, Dominique POQUILLON, Kevin CAVE reports financial support was provided by SAFRAN Aircraft Engines. Moukrane DEHMAS, Dominique POQUILLON reports equipment, drugs, or supplies was provided by DESY (Hamburg, Germany). Nothing to mention to the best of the author

Acknowledgments

Authors would like to acknowledge Mr. G. Geandier (Jean Lamour Institut – Nancy, France) and M. Fares (SLIM) for their work to perform synchrotron tests in Hamburg on our sample. Authors also acknowledge DESY (Hamburg, Germany), a member of the Helmholtz Association HGF, for the provision of experimental facilities. Parts of this research were carried out at PETRA III using beamline P21.2- The Swedish Materials Science Beamline.

References

[1] R.R. Boyer, An overview on the use of titanium in the aerospace industry, Mater. Sci. Eng. A 213 (1996) 103–114.
[2] C.E. Shamblen, T.K. Redden, Sci. Technol. Appl. Titanium, R.I. Jaffee N.E. Promisel, Air Contamination and Embrittlement of Titanium Alloys, Eds., Pergamon Press. Oxford, United Kingdom (1968) 199–208.
[3] L. Bendersky, A. Rosen, The effect of exposure on the mechanical properties of the Ti-6Al-4V, Eng. Fract. Mech. 20 (1984) 303–311.
[4] A. Casadebaigt, J. Hugues, D. Monceau, High temperature oxidation and embrittlement at 500–600°C of Ti-6Al-4V alloy fabricated by laser and electron beam melting, Corros. Sci. 175 (2020), 108875.
[5] D.P. Satko, J.B. Shaffer, J.S. Tiley, S.L. Semiatin, A.L. Pilchak, S.R. Kalidindi, Y. Kosaka, M.G. Glavicic, A.A. Salem, Effect of microstructure on oxygen rich layer evolution and its impact on fatigue life during high-temperature application of α/β titanium, Acta Mater. 107 (2016) 377–389.
[6] R.N. Shenoy, J. Unnam, R.K. Clark, Oxidation and embrittlement of Ti-6Al-2Sn-4Zr-2Mo alloy, Oxid. Met. 26 (1986) 105–124.
[7] C. Dupressoire, A. Rouaix-Vande Put, P. Emile, C. Archambeau-Mirguet, R. Peraldi, D. Monceau, Effect of nitrogen on the kinetics of oxide scale growth and of oxygen dissolution in the Ti6242S titanium-based alloy, Oxid. Met. 87 (2017) 343–353.
[8] K.S. McReynolds, S. Tamirisakandala, A study on alpha-case depth in Ti-6Al-2Sn-4Zr-2Mo, Metall. Mater. Trans. A 42 (2011) 1732–1736.
[9] I. Abdallah, C. Dupressoire, L. Laffont, D. Monceau, A. Vande Put, STEM-EELS identification of TiO X N Y, TiN, Ti 2 N and O, N dissolution in the Ti2642S alloy oxidized in synthetic air at 650 °C, Corros. Sci. 153 (2019) 191–199.
[10] R. Gaddam, B. Sefer, R. Pederson, M.L. Antti, Oxidation and alpha-case formation in Ti-6Al-2Sn-4Zr-2Mo alloy, Mater. Charact. 99 (2015) 166–174.
[11] J. Baillieux, C. Archambeau, P. Emile, D. Poquillon, Effet de la diffusion de l'oxygène sur le comportement mécanique du Ti–6Al–2Sn–4Zr–2Mo–0.1Si, CfM2015 (2015) 22–25.
[12] H.M. Gardner, P. Gopon, C.M. Magazzeni, A. Radecka, K. Fox, D. Rugg, J. Wade, D. E.J. Armstrong, M.P. Moody, P.A.J. Bagot, Quantifying the effect of oxygen on micro-mechanical properties of a near-alpha titanium alloy, J. Mater. Res. 36 (2021) 2529–2544.
[13] C.M. Magazzeni, H.M. Gardner, I. Howe, P. Gopon, J.C. Waite, D. Rugg, D.E. J. Armstrong, A.J. Wilkinson, Nanoindentation in multi-modal map combinations: a correlative approach to local mechanical property assessment, J. Mater. Res. 36 (2021) 2235–2250.
[14] D. Poquillon, C. Armand, J. Huez, Oxidation and oxygen diffusion in Ti-6al-4V alloy: Improving measurements during SIMS analysis by rotating the sample, Oxid. Met. 79 (2013) 249–259.
[15] C. Dupressoire, M. Descoins, A. Vande Put, E. Epifano, D. Mangelinck, P. Emile, D. Monceau, The role of nitrogen in the oxidation behaviour of a Ti6242S alloy: a nanoscale investigation by atom probe tomography, Acta Mater. 216 (2021), 117134.
[16] K.E. Wiedemann, R.N. Shenoy, J. Unnam, Microhardness and lattice parameter calibrations of the oxygen solid solutions of unalloyed e-titanium and Ti-6AI-2Sn-4Zr-2Mo, Met. Trans. A 18 (1987) 1503–1510.
[17] J. Baillieux, D. Poquillon, B. Malard, Relationship between the volume of the unit cell of hexagonal-close-packed Ti, hardness and oxygen content after α-case formation in Ti-6Al-2Sn-4Zr-2Mo-0.1Si alloy, J. Appl. Crystallogr. 49 (2016) 175–181.
[18] N. Vaché, D. Monceau, Oxygen diffusion modeling in titanium alloys: new elements on the analysis of microhardness profiles, Oxid. Met. 93 (2020) 215–227.
[19] J. Baillieux, D. Poquillon, B. Malard, Observation using synchrotron X-ray diffraction of the crystallographic evolution of α-titanium after oxygen diffusion, Philos. Mag. Lett. 95 (2015) 245–252.
[20] Y.T. Lee, G. Welsch, Young's modulus and damping of Ti6Al4V alloy as a function of heat treatment and oxygen concentration, Mater. Sci. Eng. A 128 (1990) 77–89.
[21] Y. Zhang, G.R. Ma, X.C. Zhang, S. Li, S.T. Tu, Thermal oxidation of Ti-6Al–4V alloy and pure titanium under external bending strain: experiment and modelling, Corros. Sci. 122 (2017) 61–73.
[22] K. Cavé, D. Texier, E. Fessler, D. Monceau, D. Poquillon, Size effect on the tensile mechanical behavior of thin Ti6242S specimens at 723 K and 823 K, Metall. Mater. Trans. A 54 (2023) 549–561.
[23] D. Nečas, P. Klapetek, Gwyddion: an open-source software for {SPM} data analysis, Cent. Eur. J. Phys. 10 (2012) 181–188.
[24] N. Vaché, Y. Cadoret, B. Dod, D. Monceau, Modeling the oxidation kinetics of titanium alloys: review, method and application to Ti-64 and Ti-6242s alloys, Corros. Sci. 178 (2021), 109041.
[25] A.M. Chaze, C. Coddet, The role of nitrogen in the oxidation behaviour of titanium and some binary alloys, J. Less-Common Met. 124 (1986) 73–84.
[26] J. Rodriguez-Carvajal, FULLPROF: a program for Rietveld refinement and pattern matching analysis, in: Satell. Meet. Powder Diffr. XV Congr, IUCr, 1990.
[27] S. Yamaguchi, Interstitial order-disorder transformation in the Ti-O solid solution. I. Ordered arrangement of oxygen, J. Phys. Soc. Japan 27 (1969) 155–163.
[28] A.L. Pilchak, W.J. Porter, R. John, Room temperature fracture processes of a near-α titanium alloy following elevated temperature exposure, J. Mater. Sci. 47 (2012) 7235–7253.
[29] L. Despax, Étude Des Mécanismes de Plasticité Lors de La Mise En Forme de l'alliage de Titane Ti-6Al-4V : Influence de La Microstructure Initiale et Des Conditions de Sollicitations Thermomécaniques, 2021.
[30] J.L. Murray, H.A. Wriedt, The O-Ti (Oxygen-Titanium) system, J. Phase Equilibria 8 (1987) 148–165.
[31] H.A. Wriedt, J.L. Murray, The N-Ti (Nitrogen-Titanium) system, Bull. Alloy Phase Diagrams 8 (1987) 378–388.
[32] A.T. Motta, L. Capolungo, L. Chen, M. Nedim, M.R. Daymond, D.A. Koss, E. Lacroix, G. Pastore, A. Simon, M.R. Tonks, B.D. Wirth, M.A. Zikry, Hydrogen in zirconium alloys: A review 518 (2019) 440–460.
[33] J. Baillieux, Effets De l'oxydation sur le Comportement Mécanique de Structures Minces en Alliages de Titane, Institut National Polytechnique de Toulouse (INP Toulouse, 2015.